

JGR Space Physics

RESEARCH ARTICLE

10.1029/2020JA028308

Key Points:

- One Equatorial Plasma Bubble (EPB) moves eastward while trailing EPB moves westward indicating unusual bidirectional drift pattern
- Large eastward drift values toward dip equatorial region as compared to low latitude region
- The diminishing of EPBs is observed due to interaction with enhanced intensity region

Supporting Information:

Supporting Information may be found in the online version of this article.

Correspondence to:

R. N. Ghodpage,
rupeshghodpage@gmail.com

Citation:

Ghodpage, R. N., Gurav, O. B., Taori, A., Sau, S., Patil, P. T., Erram, V. C., & Sripathi, S. (2021). Observation of an intriguing equatorial plasma bubble event over Indian sector. *Journal of Geophysical Research: Space Physics*, 126, e2020JA028308. <https://doi.org/10.1029/2020JA028308>

Received 4 JUN 2020

Accepted 19 MAR 2021

Observation of an Intriguing Equatorial Plasma Bubble Event Over Indian Sector

R. N. Ghodpage¹ , O. B. Gurav^{2,3}, A. Taori⁴, S. Sau^{2,5} , P. T. Patil¹, V. C. Erram¹, and S. Sripathi² 

¹Medium Frequency Radar Facility, Indian Institute of Geomagnetism, Kolhapur, India, ²Indian Institute of Geomagnetism, Navi Mumbai, India, ³Now at: Department of Physics, Bharati Vidyapeeth (Deemed to be University), Yashwantrao Mohite College of Arts, Science and Commerce, Pune, Maharashtra, India, ⁴National Remote Sensing Centre, Hyderabad, India, ⁵Arecibo Observatory, Puerto Rico, USA

Abstract We report an interesting Equatorial Plasma Bubbles (EPBs) event during the night of March 22–23, 2017. To investigate the dynamics of observed EPBs, we utilize multi-instrument data obtained with all-sky imager (ASI) from Panhala (16.48°N, 74.6°E, 11.1°N Dip. Lat.), Canadian Advanced Digital Ionosonde (CADI) from Tirunelveli (8.73°N, 77.7°E, 1.6°N Dip. Lat.) and ionospheric backscatter echoes data of Gadanki Ionospheric Radar Interferometer (GIRI) radar from Gadanki (13.5°N, 79.2°E, 6.5°N Dip. Lat.) over Indian regions. The optical observations from Panhala reveal clear signatures of EPBs from ~1600 UT onwards and corresponding ESF occurrence is noted in CADI at Tirunelveli as well. Backscatter echoes are also recorded in Range time intensity map obtained by GIRI after ~17:45 UT. On this night, two EPBs (EPB1 and EPB2) are observed with inter-depletion distance of ~600 km. The EPB1 drifts eastward throughout the night and evolves with time as bifurcated structures while the trailing EPB2 drifts eastward initially and eventually drifts westward. We believe that this is the first evidence of differential drifts of EPBs imaged through ASI over a narrow longitudinal zone over the Indian region.

1. Introduction

Ionospheric irregularities are frequently generated at F-region during post-sunset period over the equator through Rayleigh-Taylor (RT) instability. RT instability gives rise to a hierarchy of irregularities of scale sizes from few cm to hundreds of km whose signatures are termed as Equatorial Spread-F in ionograms or plasma plumes in radars (e.g., Kelley, 1989; Kelley et al., 2011; Patra et al., 2014). In optical data, they are named as Equatorial Plasma Bubbles (EPBs) and are manifestation of large-scale plasma irregularities. EPBs grow nonlinearly at the equator and simultaneously get mapped to low latitudes along the magnetic field lines (e.g., Makela & Otsuka, 2011). OI 630.0 nm airglow imaging captures the nightglow emission which arises from the dissociative recombination of O₂⁺ with electron and has peak emission altitude at ~250 km (e.g., Sahai et al., 2006). The dark, field aligned bands observed in the OI 630 nm images are manifestation of electron density bite outs representing the occurrence of EPBs. Such structures have been previously imaged at low latitude stations using optical techniques (e.g., Martinis et al., 2018; Taori et al., 2013).

Many researchers have studied the dynamics of EPBs in the context of their zonal drifts, occurrence statistics, morphological evolution etc (e.g., Chian et al., 2018; Gurav et al., 2019; Kakad et al., 2017; Sharma et al., 2017 etc.). The EPBs frequently occur in high solar activity but during low solar activity period a stronger perturbation is needed for their development (e.g., Buhari et al., 2017) which could either be of wave-like seed of lower atmospheric origin (e.g., Taori et al., 2011) or of electrical origin such as magnetic disturbance (e.g., Sripathi et al., 2018). Usually, EPBs drift eastward during the night time (e.g., Taori & Sindhya, 2014) with peak magnitude before mid-night and magnitude of drift decreases toward the dawn period but sometimes EPBs move westward during the night. The westward drifts are caused mainly due to the magnetic disturbances (e.g., Patra et al., 2016; Sau et al., 2017). Abdu et al. (2003) observed intense plasma bubbles in the Brazilian sector during interplanetary magnetic field (IMF Bz) southward turning associated with Auroral Electrojet Indices (AE) intensification. In that study, due to such magnetic disturbances, the height rise of the F-layer was noted to be accompanied by increased eastward electric field. Candido et al. (2019) observed unusual spread F structures using ionosonde and optical all-sky imager (ASI) over Brazilian sector during mid-night to post-midnight hours of moderate solar activity conditions. Their

results show that plasma irregularities (EPBs) were moving westward in its occurrence time. Further their studies on neutral wind analysis using Fabry–Pérot interferometer reports that gravity wave propagation at ionospheric heights could have influenced the post-mid night RT instability favoring the generation of EPBs. Sobral et al. (2011) studied the westward drifting EPBs using airglow imager data over Brazilian sector on 14 quiet days during the period 2001–2006. They found that the frequency of occurrence of westward drifting EPBs increases toward descending phase of the solar cycle. They have observed the drift speed of EPBs between ~ 20 and 40 m/s. In the months of July–September, the occurrence of westward drifting EPBs was maximum. The westward drifting EPBs were not observed between November and April during the period under their study. They finally concluded that the westward thermospheric wind are main drivers behind the westward drifting EPBs. Paulino et al. (2010) studied westward drifting EPBs over Brazilian sector using optical observations of the OI 630 nm airglow emission under quiet or weak magnetic periods concluding that the intense magnetic disturbance is not the only reason for westward drift of EPBs. Huba et al. (2015) studied EPBs merging process using ASI data and SAMI3/ESF model and observed that electrostatic potential associated with one EPB can connect with that of adjacent EPB and merges with it through electrostatic reconnection process. Kakad et al. (2017) studied zonal irregularity drift during magnetically disturbed conditions using spaced receiver system over Indian region and suggested that westward drifts were linked with the magnetic activity are smaller at the low latitudes as compared to the dip equator. Ghodpage et al. (2018) calculated zonal drift of EPBs using all-sky image data recorded over Kolhapur during storm day of March 17, 2015 and found that EPBs move westward with drift velocity as low as -70 m/s. They concluded that this westward drift is caused by the presence of disturbance dynamo electric field apart from prompt penetration during the storm day. From the same location, Gurav et al. (2018) investigated zonal drift of EPBs on magnetically disturbed night using ASI and observed that the EPBs have different drifts along the meridian. Xiong et al. (2018) studied EPBs using ASI and SWARM satellite data and observed that the bifurcation of EPBs occurred firstly at the higher latitudes and then observed at lower latitudes. The secondary branches observed during this bifurcation show very thinner structures with 20 – 30 km east-west extension and later started merging with each other which resulted into complicated mesh of EPBs.

In spite of a number of investigations, the EPB events show large degree of variability from one event to other and factors behind their onset are often so enigmatic that several attempts have been made to understand them by several groups throughout the world. This study reports an intriguing observation of EPB events investigated using multi-instrument observations over the Indian region in which drift of one EPB was found to reverse from eastward to westward while other leading EPB continued its eastward drift.

2. Details of the Instruments Utilized

In this work we use three instrument data namely ASI at Panhala, VHF radar at Gadanki and ionosonde at Tirunelveli.

2.1. All-Sky Imager at Panhala

One ASI is installed by Indian Institute of Geomagnetism (IIG) at MF Radar Facility, Shivaji University campus, Kolhapur (SUK) under the scientific collaborative program between IIG and SUK. In the present study, this ASI is operated from Panhala (16.48°N , 74.6°E , 11.1°N Dip. Lat.) which is ~ 25 km west to Kolhapur and ~ 800 m above the mean sea level. Panhala is a better place for nightglow observations as it lies on a hill station and has less light as well as dust pollution. Our ASI consists of a high resolution [$1,024 \times 1,024$ pixels (i.e., 1 MP)] CCD and has 180° field of view (FoV). But the images used for the current study are processed with 140° FoV which covers an area of $\sim 1,200$ km in diameter at 250 km altitude. The integration time for ASI imager is ~ 120 s. Comprehensive information of the ASI is described in Gurav et al. (2019). ASI raw image data are processed and unwrapped to equidistant projection assuming an emission altitude of 250 km as described in Narayanan et al. (2009). The zonal drifts of EPBs imaged in ASI data have been calculated by examining their longitudinal offset in meters following Pimenta et al. (2001).

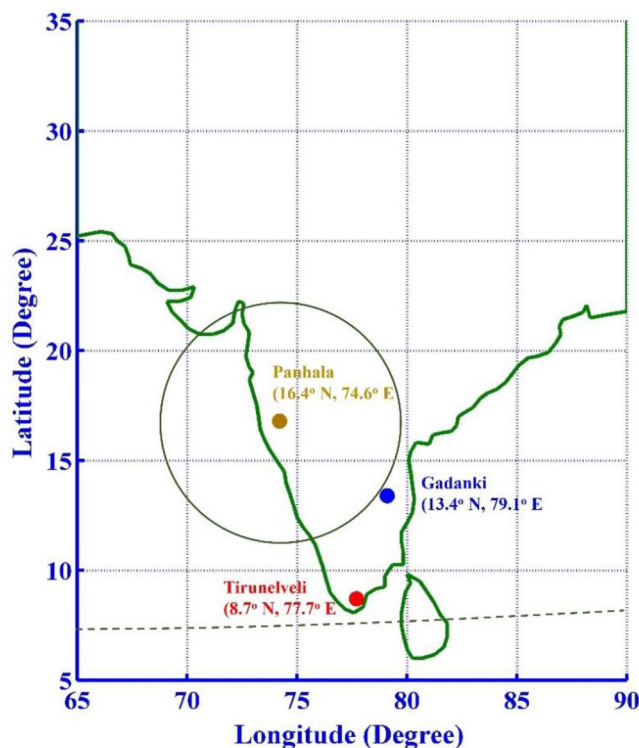


Figure 1. This Figure shows the locations of all-sky imager (ASI), Gadanki Ionospheric Radar Interferometer and ionosonde at Panhala, Gadanaki and Tirunelveli respectively. The circle drawn around Panhala location depicts the field of view of all-sky imager which is 140° covering area of about ~1,200 km in diameter. The green dotted line indicates dip equator.

2.2. Canadian Advanced Digital Ionosonde at Tirunelveli

We also utilize here Canadian Advanced Digital Ionosonde (CADI) data recorded from Tirunelveli (8.73°N, 77.7°E, 1.6°N Dip. Lat.) which is a dip equatorial station in India. It works in both frequency scanning and fixed frequency modes. Its frequency range is between 1 and 20 MHz and can be operated with different temporal resolution. It consists of a delta type antenna along with the four receivers mounted east-west and magnetic north-south direction which is capable of measuring the irregularity drift in east-west as well as north-south directions. CADI at Tirunelveli is a powerful tool in the context of probing the equatorial ionosphere and its electrodynamics. The system description and its feature in detail can be found in Sripathi et al. (2016).

2.3. Gadanki Ionospheric Radar Interferometer at Gadanki, Tirupati

We have utilized Gadanki Ionospheric Radar Interferometer (GIRI) data taken from Gadanki (13.5°N, 79.2°E; 6.5°N Dip. Lat.), an off equatorial location of India. It works at both 30 and 50 MHz frequencies which is essential to examine the bottom as well as topside irregularities of the ionosphere. This system also gives the Doppler velocity, spectral width and drift variations of small-scale irregularities. The radar beam is directed perpendicular to the magnetic field lines to detect the backscatter from the field aligned irregularities. To achieve this, the dipoles of the radars are oriented at 14° inclination angle with respect to the horizontal. This particular inclination angle is chosen for the dipoles as the antenna gain is maximum at 14° inclination for this location. During the EPB event discussed in this work, beam scanning was not performed, instead the beam was directed at 10° west azimuth. As a result, the beam would point at a location which is ~53 km west of Gadanki longitude at 300 km altitude. In another word, during the event reported in this study, GIRI was pointing at a location that is ~470 km east of Panhala longitude at 16° geographic latitude. The GIRI system details are exclusively described in Patra et al. (2014).

3. Results and Discussion

The locations of the different instruments used in this study over the Indian sector are depicted in Figure 1. The sequential nightglow images obtained in OI 630.0 nm emission on the night of March 22–23, 2017 are shown in Figure 2. These are the processed and unwrapped images having 140° FoV. The spatial scales pertaining to the observations are marked in the first image, while, the vertical and horizontal white strips marked in the second image are for the keogram analysis to investigate the latitudinal and longitudinal variability, respectively. During this night, we observed several EPBs. The two EPBs which are most prominent and are main focus of this study are marked as EPB1 (yellow arrow) and EPB2 (red arrow). The first EPB that appeared in the images around 1,600 UT is henceforth referred as EPB0 for the sake of easy understanding. EPB0 drifts eastward between 1,600 and 1,730 UT and after that, it got diminished and could not be clearly identified. Afterward, another three EPBs appeared between EPB0 and EPB1. One of these EPBs is situated very close to EPB1 and to the east of it. All these three intermediate EPBs between EPB0 and EPB1 are seen to move eastward. They have not been analyzed in detail, as they are not the focus of this study. The EPB1 exhibits growth in the apex altitude between 1,641 and ~19:30 UT while drifting to the east. Around 1,930 UT, EPB1 reached the northmost limit of our ASI FoV. Afterward, it might have propagated to higher apex altitudes which could not be ascertained from our images. At ~1,700 UT, EPB1 starts bifurcating with poleward expansion suggesting that EPB developed to very high altitudes. These structures (i.e., EPB1) got diminished after ~2,153 UT. On the other hand, EPB2 started appearing into the FOV at

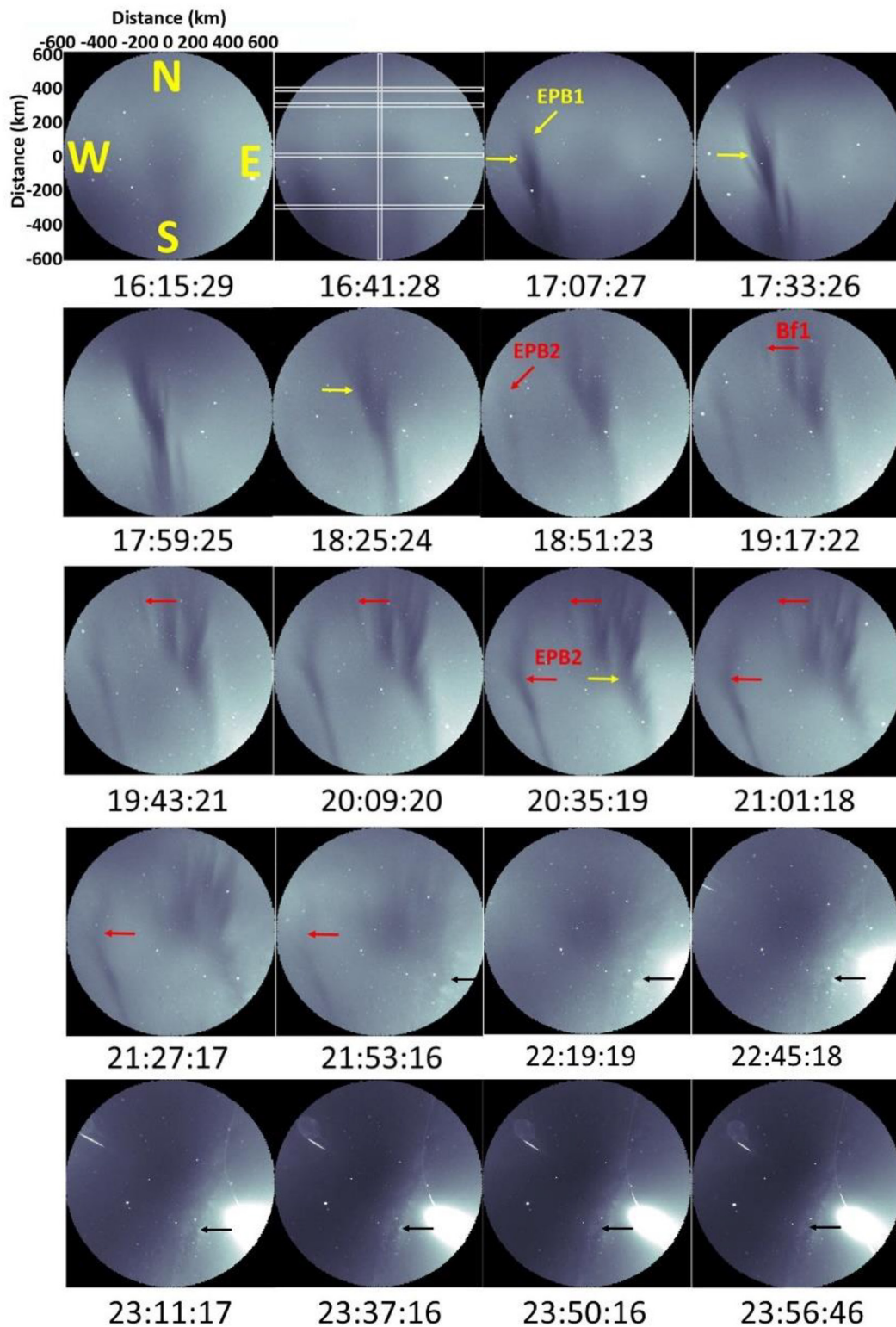


Figure 2. Sequences of unwrapped images with 140° field of view during the night of March 22–23, 2017. Approximately every fifth image collected on this night is shown in this figure. The yellow and red marked arrows depicts Equatorial Plasma Bubbles (EPBs) with different zonal drifts. The time shown at the bottom of each image is in UT. The east-west and north-south distance in kilometer is shown in first image at 16:15:29 UT. The vertical and horizontal strips of size 20 pixels to obtain north-south and east-west keograms respectively are shown in second image at 16:41:28 UT. The bright region in last couple of images depicts the local moon entrance and the black arrows indicate the direction of milky way galaxy.

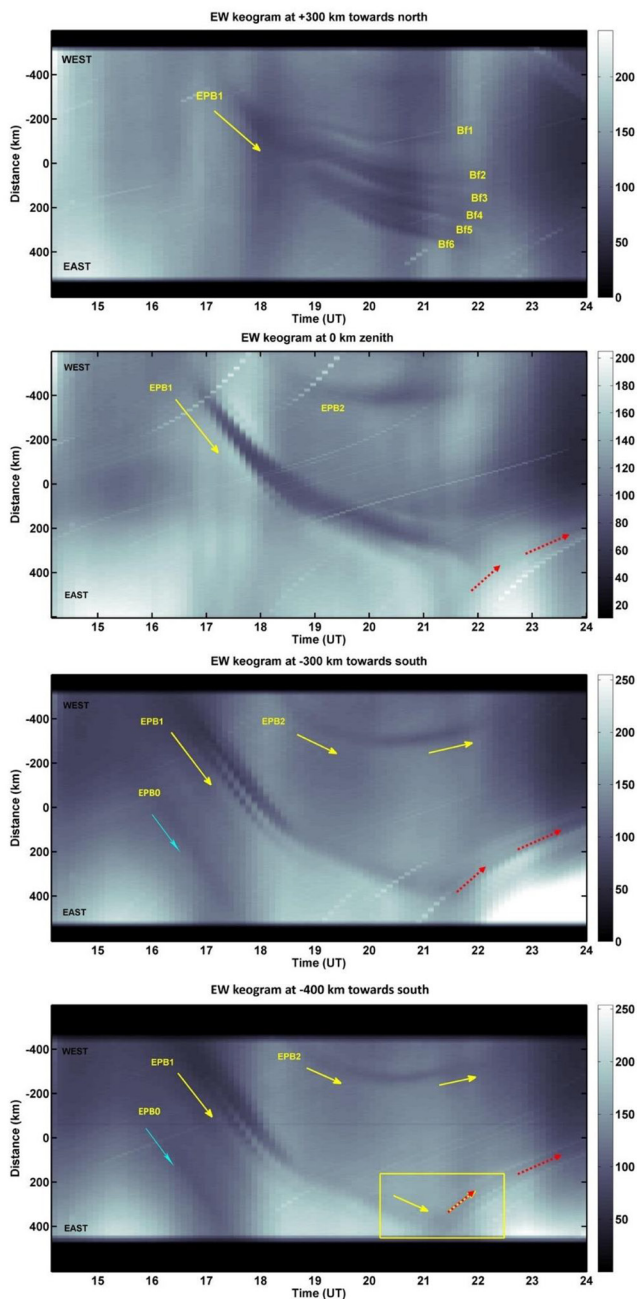


Figure 3. East-west keograms plotted at (a) +300 km north, (b) at 0 km i.e., at Zenith and (c) at -300 km south and (d) at -400 km south during the night of March 22–23, 2017. The yellow and cyan arrows indicate the direction of Equatorial Plasma Bubbles (EPBs). The red dotted arrows indicate the westward motion of Milky Way galaxy.

~18:30 UT as shown by red arrow in Figure 2. At around 19:17 UT, EPB1 and EPB2 had a separation of about ~600 km at zenith. It is noted that, similar to the EPB1, EPB2 also diminished after ~21:53 UT.

To understand the EPB characteristics (drift velocity and intensity variability), we carry out keogram analysis. The drift velocity is calculated by taking an east-west slice of 20 pixels of ASI images at zenith as well as ± 300 km to the north and south of zenith as shown in Figure 2 (Ref. image of 1,641 UT). The east-west keograms obtained from different latitudes are depicted in Figure 2. In the keograms, motion of EPB0 is marked with a cyan arrow. In Figure 3c we notice that EPB1 at -300 km south ($\sim 14.07^\circ\text{N}$ geographic) commenced at $\sim 16:45$ UT which is shown by a yellow arrow. Initially, we see only one EPB arm drifting eastward but after $\sim 17:00$ UT it starts bifurcating and forms finger like structures. We have denoted these bifurcations as Bf1–Bf6, which are marked in Figure 3a. All these bifurcated structures drift eastward except the end portion of Bf1 which has little westward drift. This is further elaborated in Figure 4a. With regard to Figure 3b, we note the existence of two EPBs, i.e., EPB1 and EPB2. EPB1 starts appearing at $\sim 16:41$ UT and ~ 2 h later around 18:30 UT, EPB2 appears in the images. From Figures 3b and 3c, it is observed that, EPB2 shows clear eastward drift from 18:30 to $\sim 20:00$ UT and after 20:00 UT, EPB2 starts drifting westward. It is evident from Figure 3 that EPB1 and most of its bifurcated structures drifts eastward throughout the night. This indicates that there is a strong variation in drifts within the narrow longitude extent of the images. Another thing to note is that the inter-depletion distance between these two EPBs starts increasing with time which may be due to the reduced drift velocity and subsequent reversal of drift of EPB2 as the time progresses.

In Figure 3d, we have marked a portion with a yellow rectangle. Here it appears that some depleted structure is moving westward after $\sim 21:15$ UT. We have marked this westward motion with red dotted arrows in Figures 3b–3d. Similarly, if we look at Figures 3b and 3c, it appears that some depleted structure is moving westward after $\sim 21:30$ UT. After carefully comparing occurrence period of this westward drift in the images, we find out that these depleted structures were actually signature of the Milky Way galaxy and not associated with any EPBs. From the images shown in Figure 2, it can be apparently noticed that the Milky Way galaxy is appearing from the southeast corner (Ref. black arrows shown in Figure 2 after $\sim 21:00$ UT which are drifting westward). It is also evident from the images that after $\sim 21:30$ UT, the portion of EPB1 situated to the south of -300 km south is not clearly visible. This could be partly due to the presence of the Milky Way galaxy in that part of the images or partly due to the process of diminishing of EPB1 into the background. However, Figures 3b–3d shows that some intensity depleted structure was moving westward till 24:00 UT and may be beyond that as well. This confirms our assumption that this westward movement is associated with the Milky Way galaxy and not with EPB1. Therefore, we confirm that the main trunk of EPB1 and most of its bifurcations (except Bf1) does not show any westward drift on this night.

To estimate the drift velocity, we used scanning method which was described by Pimenta et al. (2001). We inferred zonal drifts of these EPBs at different latitudes i.e., +300 km north ($\sim 19.5^\circ\text{N}$), 0 km i.e., zenith ($\sim 16.8^\circ\text{N}$) and -300 km to south ($\sim 14.07^\circ\text{N}$). The drift velocity thus calculated are shown in Figure 4a–4c, respectively. In Figure 4a, it is seen that EPB1 and its fingerlike structures move eastward until $\sim 21:30$ UT.

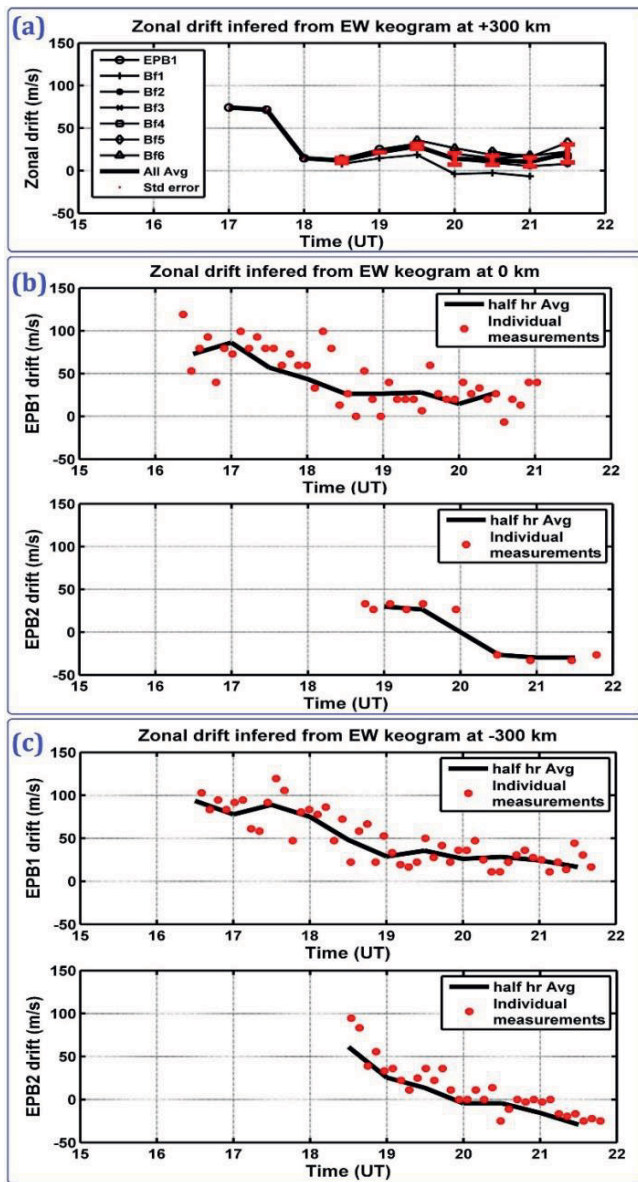


Figure 4. (a) shows half hour averaged zonal drifts of all Equatorial Plasma Bubbles (EPBs) marked in keogram (a) which are measured at +300 km. The individual measurements of their drifts are not shown here, (b) shows half hour averaged (black line) zonal drift of EPB1 and EPB2 measured at 0 km. The red points are the individual measurements and (c) shows half hour averaged (black line) zonal drift of EPB1 (top panel) and EPB2 (bottom panel). The red points in top and middle panel are the individual measurements.

Only Bf1 show a weak westward drift after ~20:00 UT as can be observed in Figure 4a. We note that the drift velocity of EPB1 is in the range of 100 to 25 m/s between 16:00 and 20:00 UT which compares well with the drift values reported by Taori and Sindhya (2014). Further, we also note a step like variation in the drift pattern after 17:30 UT (Ref. Figure 4a) which indicates the presence of strong gradients in the drift velocity. Figure 4b shows the zonal drifts of EPB1 (top panel) and EPB2 (bottom panel). This plot shows that EPB2 slows down its eastward drift after 19:30 UT and eventually drifts westward after 20:00 UT, while EPB1 continue its eastward drift (top panel of Figure 4b). Similar drift pattern of EPB1 and EPB2 can be clearly noted in Figure 4c as well.

We tried to examine this differential nature of the drift velocity. Figure 5 shows the drift velocity estimated for the finger-like structures Bf1–Bf6 associated with EPB1 and are denoted as DV1..., DV6 etc. Upward tick arrows show that drifts were eastward while the downward tick arrows show westward drift. Shown together with the ticks are the duration of the noted bifurcation. We can see that drift velocity in general reduces as the longitude decreases. This suggests that EPB2 had external effects on its polarized electric field more than the EPB1. This is understandable from the view that EPB movements in general are a combined impact of vertical electric field inside the bubble arising due to plasma polarization and background zonal (horizontal) electric fields. However, the polarization field inside EPB is upward; this means that the plasma inside EPB experiences two vertical field: downward field due to background dynamo and upward field due to polarization. As a result, EPB always moves westward with respect to background plasma (Mukherjee et al., 2014; Tsunoda et al., 2018). In general, when the EPB height is high, polarization electric field is small and when EPB height is low, polarization is high. Therefore, the effects of polarization electric field variation would be significantly larger on EPB2 than EPB1. In nutshell, along with EPB2, one branched structure of EPB1 (i.e., Bf1) has also changed its direction to west afterward. So, some influence of DDEF is also there on Bf1 which is why it drifted to west similar to the trailing EPB2.

To supplement the above EPB occurrences in optical data we investigated the CADI ionosonde data at an equatorial station, Tirunelveli. The occurrences of ESF are noted in the ionograms at Tirunelveli around 16:30 UT (22:00 IST) which supports the observation of EPBs in image data acquired over Panhala. In Figure 6, panel (a) depicts h'f variation on the event day along with its variation on five international quiet days of March 2017; panel (b) and (c) shows the IMF Bz and IEF variations during the night of March 22–23, 2017, respectively. Note that h'f increased from about 200 to 325 km before the occurrence of EPBs on March 22–23, 2017. As mentioned earlier, IMF Bz show quasi periodic variation between 10:00 and 16:00 UT which is reflected in the corresponding fluctuations in F-layer as can be seen by magenta curve. These quasi-periodic oscillations could be the manifestation of some seeding sources of the RT

instability or the magnetic disturbance accompanied by IMF Bz fluctuations onto the ionospheric parameters. The upward (downward) motion of the F layer observed in the ionosonde data (h'f variation) may be attributed to the eastward (westward) penetration electric field on this night. Sripathi et al. (2018) observed the generation of post-midnight EPBs around mid-night to dawn sector on February 04–05, 2011 due to the eastward penetration of electric field accompanied by southward IMF Bz turning. The southward turning of IMF Bz around mid-night to pre-sunrise period has produced eastward penetration electric field which caused the F-layer height enhancement which eventually favored the generation of EPBs. In the present

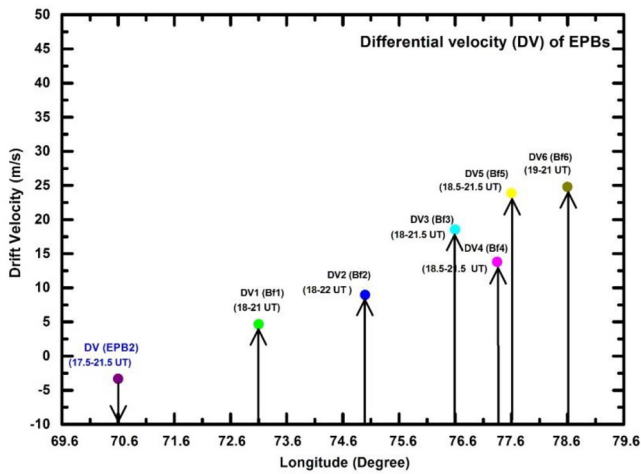


Figure 5. Shows the differential velocities of Equatorial Plasma Bubble 2 (EPB2) and bifurcated structures of EPB1 namely Bf1, Bf2, Bf3, Bf4, Bf5 and Bf6 with respect to longitudes. The downward arrow shows the westward motion while upward arrow shows the eastward motion. The length of the arrow gives the average magnitude of the drift velocity.

case also, F layer height has increased possibly due to eastward penetration electric field accompanied by southward IMF Bz turning around pre-midnight hours. The maximum height rises up to ~ 325 km is seen during this disturbed night when IMF Bz has sharp southward turning around 16:00 UT (22:30 IST). Just after few minutes ESF occurrence is noted in ionosonde with corresponding signatures of EPBs in ASI over Panhala. The generation of irregularities is possibly associated with the eastward penetration of electric field accompanied by southward IMF Bz turning. Figures 7a and 7b show the iso-frequency and iso-heights obtained from CADI data recorded at Tirunelveli. From the iso-frequency lines it is seen that there are two prominent wavy features, one at $\sim 11:00$ UT and other at $\sim 15:00$ UT before the spread F occurrence. The approximate periodicity of these wavy features (~ 4 h) is larger than the fluctuations of IMF Bz. This indicates that there could be a possibility of bottom side seed perturbation at equatorial region which is in conformity with the observations noted by Patra et al., (2013). It is further seen that during the spread F occurrence period the layer is going up simultaneously and exhibits the third prominent peak around $\sim 17:30$ UT. Another thing to note here is that the F layer vary between 200 and 300 km during the time interval from 18:00 to 22:00 UT. It is believed that the airglow

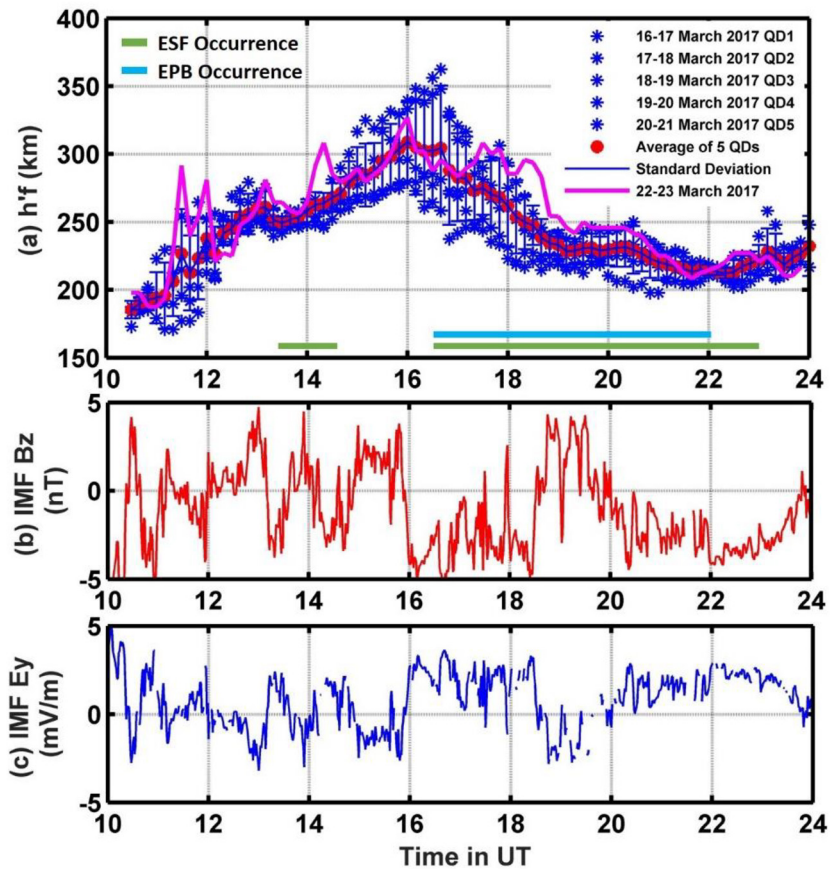


Figure 6. (a) The $h'f$ variation during disturbed night March 22–23, 2017 (magenta line) along with its variation on five international quiet days with the mean (solid red curve) and standard deviation (vertical blue bars) are also shown. The green and cyan horizontal strips indicate the ESF/EPB occurrences inferred from Canadian Advanced Digital Ionosonde (CADI) (Tirunelveli) and all-sky imager (ASI) (Panhala) respectively. (b) The interplanetary magnetic field and (c) Interplanetary electric field E_y variations during the night of March 22–23, 2017.

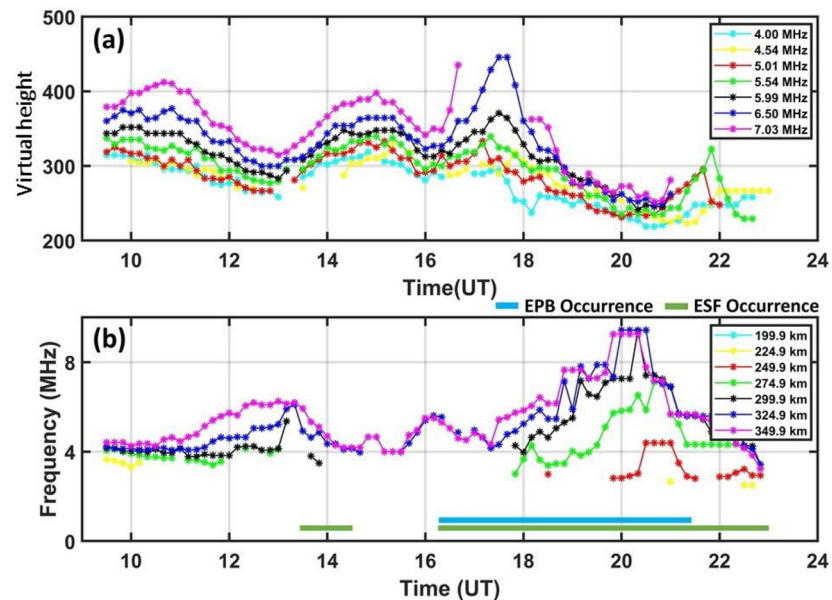


Figure 7. (a) The temporal variation of isodensity undulations of ionosonde F region observations which is at fixed (frequencies) over Tirunelveli (b) The temporal variation of isoheight undulations of ionosonde F region observations, which is at fixed (virtual heights) altitudes over Tirunelveli, the green and cyan horizontal strips indicates the ESF/EPB occurrences inferred from Canadian Advanced Digital Ionosonde (CADI) (Tirunelveli) and all-sky imager (ASI) (Panhala) respectively during the night of March 22–23, 2017.

emission peak altitude occurs around $\sim 250 \pm 50$ km, which is why one can see clear signatures of ionospheric irregularities in airglow images during the period where F-layer altitude is around ~ 250 km. From the iso-height plots it is seen that larger frequencies have reflected from the dense ionosphere between 18:00 and 22:00 UT where the peak density of the layer varied from 200 to 300 km.

Further, to investigate whether EPBs observed in the images were active, we look at the VHF radar observations made at Gadanki which is located to the southeast of Panhala but having nearly similar latitude. In Figure 8, Panel (a, b, and c) indicates Height-time variations of SNR (dB), Doppler velocity (m/s) and Spectral width (m/s) obtained using VHF radar over Gadanki during the period of March 22–23, 2017, respectively. The presence of backscatter echoes during 17:45–20:00 UT suggests that irregularities associated with EPBs occurred at ionospheric altitudes. Spectral width of GIRI is estimated as twice of the square root of velocity variance. The growth and decay of EPBs can be attributed to increasing and decreasing values of spectral widths, respectively. Positive (negative) velocity represents irregularity velocity away from (toward) the radar. Large spectral widths are generally associated with field aligned irregularities EPBs typically observed during post-sunset period and small spectral widths with values as low as 10 m/s can be observed during the late-night hours (Patra et al., 2014). During the presence of backscatter echoes on March 22–23, 2017, GIRI exhibits positive velocities only (Figure 8c). This implies that the EPB observed by GIRI was continuously moving away from Gadanki. In addition, Doppler velocity of the observed EPB is positive initially indicating upward movement and growth of the EPB. The Doppler velocity turned marginally negative after 19:30 UT (01:00 IST) suggesting the decay of EPB (Figure 8b).

Now we consider different possible scenarios regarding the EPB observed by GIRI. It is possible that one of the EPBs observed in the images acquired from Panhala might have traveled into the FoV of GIRI. After carefully examining the airglow images, we observe that EPB0 propagated very close to the FoV of GIRI (i.e., ~ 470 km east of Panhala longitude) around 17:30 UT but as mentioned earlier, EPB0 got diminished by the same time. It is very unlikely that EPB0 would have revived afterward and then detected by GIRI as a growing EPB. Another important point is that EPB0 was traveling toward GIRI and not away from it. As already mentioned earlier, all the three EPBs that appeared between EPB0 and EPB1 traveled eastward and all of them diminished before reaching the FoV of GIRI. At 20:00 UT, EPB1 is situated ~ 300 km east of Panhala longitude (Figure 2) and moving eastward (Figure 4). Thus, EPB1 did not appear within the FoV

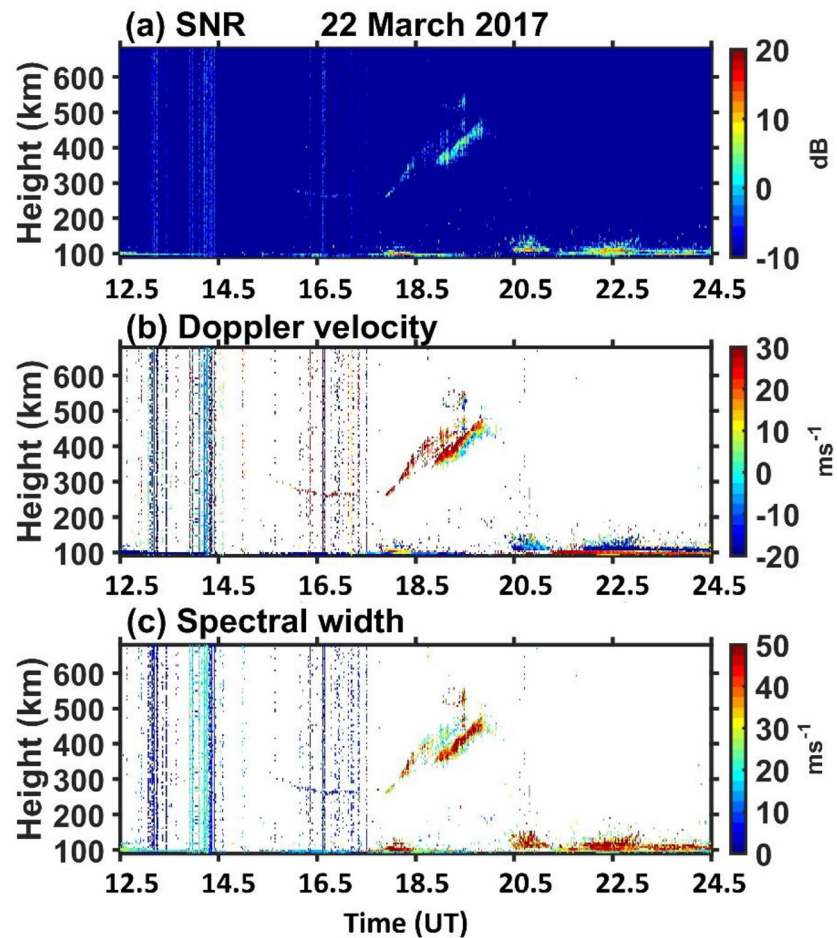


Figure 8. The temporal variations of (a) Height-time variations of SNR (dB), (b) Doppler velocity (m/s), (c) Spectral width (m/s) obtained using VHF radar over Gadanaki during the period of March 22–23, 2017.

of GIRI between 17:45 and 20:00 UT. The other possibility is that an EPB might have freshly generated very close to longitude of GIRI around 17:45 UT. Now, if this EPB travel toward west with respect to GIRI then it should appear in the Panhala images as a westward moving and growing EPB. We do not observe any such EPB within the image FoV and to the east of Panhala between 17:45 and 20:00 UT. Therefore, we conclude that none of EPBs observed in the Panhala images could cause the backscatter echoes observed by GIRI. Most likely, it was a freshly generated EPB that evolved very close to the longitude of GIRI and traveled to the east of GIRI with time.

The sequence of events discussed above shows that a strong longitudinal gradient in zonal drifts possibly associated with magnetic disturbance existed within a narrow longitudinal zone of $\sim 5.4^\circ$ over Indian region on March 22–23, 2017. It appears that a sharp boundary was present close to the longitude of Panhala. EPB2 and Bf1 are located to the west of the boundary while all other EPBs (i.e., EPB1 and its other bifurcations) are to the east of it. To the east of this boundary the drifts are eastward throughout the night while to the west of the boundary drifts reversed from eastward to westward after $\sim 20:00$ UT. We believe that only EPB2 and Bf1 have responded to disturbance dynamo electric field while EPB1 and Bf2–Bf6 are not influenced by this effect and hence kept drifting eastward throughout the course of the night. To our knowledge, such a scenario has not been reported to date by using ASI and that makes this present work interesting. At present, we are unable to explain how such a sharp gradient in the zonal drift of EPBs may occur in response to the disturbed dynamo electric fields. This observation warrants further investigation into the causative mechanism.

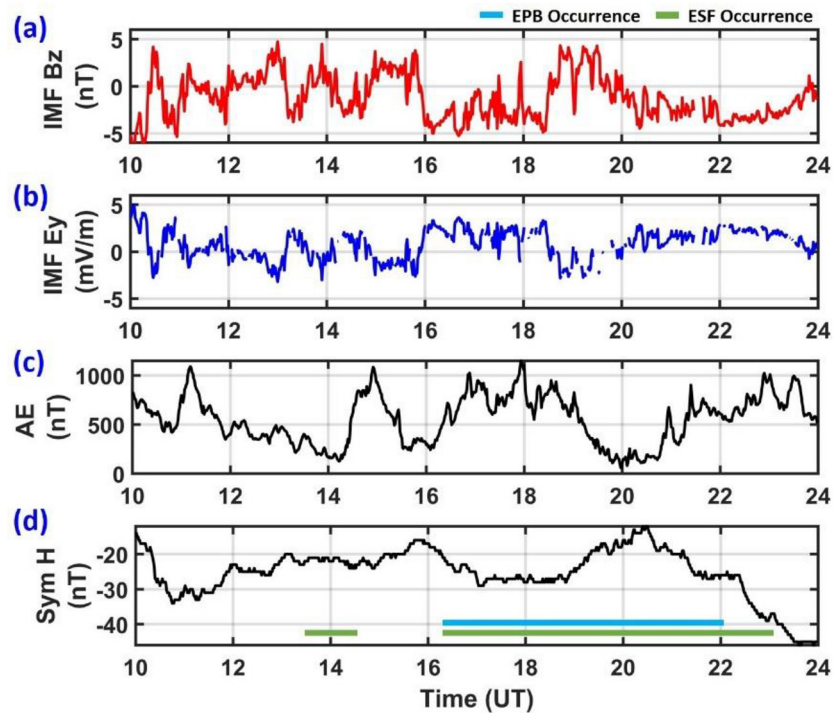


Figure 9. Temporal variation of (a) interplanetary magnetic field B_z (nT) (b) interplanetary electric field E_y (mV/m) (c) Auroral Electrojet Indices (AE) index and (d) Sym-H (nT) during March 22–23, 2017, the green and cyan horizontal strips indicates the ESF/EPB occurrences inferred from Canadian Advanced Digital Ionosonde (CADI) (Tirunelveli) and all-sky imager (ASI) (Panhala) respectively.

There are several reports in the literature explaining the causative mechanisms of westward drift of EPBs. In majority of the reports, such a transition from eastward drift to the westward is attributed to the geomagnetic storms (e.g., Abdu et al., 2012; Fejer et al., 1991; Kakad et al., 2017; Patra et al., 2016). Most commonly, the westward drift is attributed to the disturbance wind produced due to the joule heating at the high latitudes or prompt penetration of disturbance electric fields from high to the low latitudes. Kakad et al. (2017) reports that the westward drifts are stronger at the dip equatorial region as compared to low latitude station. In present study, we have not observed such effect as far as westward motion of EPBs is concerned. But, for eastward motion of EPBs, we do observe little gradient in drifts from + 300 km north to –400 km south regions (Please Ref. EPB1 eastward motion in Figures 3 and 4). We observed drift reversal after 19:30 UT over Panhala prior to that AE intensification is evident as can be seen from Figure 9. The intensification in AE is also evident during southward IMF B_z along with Sym H development state. Figure 9 shows the interplanetary parameters such as (a) IMF B_z , (b) IEF, (c) AE and (d) Sym H for the night of March 22–23, 2017. In between 1,000 to 1,016:00 UT IMF B_z shows quasi-periodic fluctuations. Around 16:00 UT IMF B_z show sharp southward turning reaching as low as –5 nT and further persisted southward up to 18:30 UT. This might set up the disturbance dynamo which is ultimately responsible for westward drifts at lower latitudes. As stated earlier that an external electric field impact may have more effect on the EPB2, a small IMF B_z penetration would have profound impact on the EPB2 drift velocity causing the reversal. Overall, effect of this disturbance dynamo is seen to be highly confined in its longitudinal extent in the Indian region and this has been imaged two dimensionally in all-sky images obtained from Panhala.

Another peculiar feature observed on the night of March 22–23, 2017 is the diminishing of EPBs. Note that in Figure 2 it is evident that EPB1 starts growing and bifurcating simultaneously as time progress. This growth can be attributed to the polarization electric field present inside the EPB. Further, after 21:53 UT both EPB1 and EPB2 seem to diminish toward the dawn period. To understand the airglow intensity (in turn, the electron density) variation, we plot north-south keogram using ASI images recorded on this night as shown in Figure 10. From the beginning of observations up to 17:30 UT, a bright intensity region is seen to move from north to south side i.e., from lower latitudes to the dip equator. This is shown by black slanted

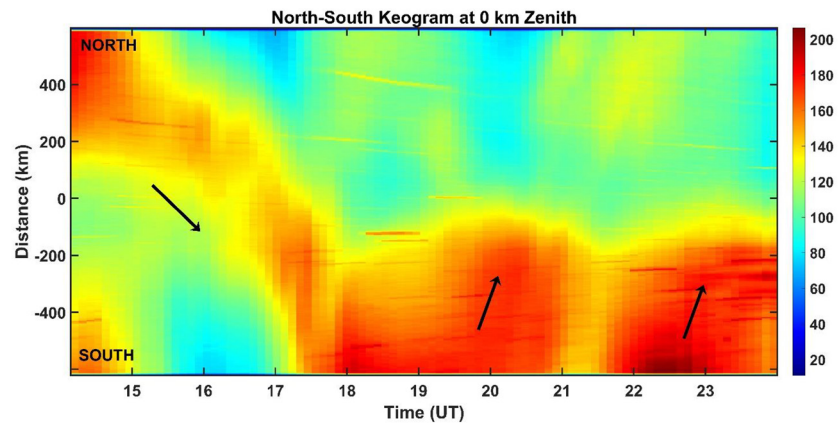


Figure 10. North-south keogram through zenith (0 km) for the night of March 22–23, 2017. The first black arrow from north to south indicates the motion of reversal in equatorial ionization anomaly (EIA). The second black arrow from south to north indicates the propagation of some bright intensity anomaly. The third black arrow from south to north indicates the enhanced airglow intensity due to local moon light condition.

southward arrow in Figure 10. This enhanced intensity region is attributed to the reversal in equatorial ionization anomaly (EIA) which appears due to the electric field reversal from eastward to westward in the night time. Such features are previously reported by many researchers (e.g., Sridharan et al., 1993). Narayanan et al. (2013) extensively described the method to calculate the drift speed of reversal EIA using OI 630.0 nm airglow images. They found average drift speed of reversal EIA to be ~ 52 m/s and also shows that the drift speeds are relatively smaller during disturbed nights as compared to quiet nights. Further, in Figure 10, two humps of bright intensity regions around 20:00 and 23:00 UT are prominently observed. Their direction is shown by black slanted arrows pointing toward north side. Please note that the enhanced region around 23:00 UT is due to the local moon light condition in early morning hours. But, the enhanced region around 20:00 UT is indeed a physical phenomenon happening at the ionospheric altitudes. One of the possibilities is that, this phenomenon could be a midnight brightness wave associated with midnight temperature maximum. The second possibility is that it may be some anomaly which is generated at the equator and traveled altitudinally (latitudinally) which eventually caused diminishing of EPBs. The EPBs are the regions of depleted density which could be filled by the interaction of such enhanced density regions. To our knowledge such diminishing of EPBs has not been reported earlier. However, Otsuka et al. (2012) found that the EPBs disappeared after the interaction with MSTIDs. They suggest that the depleted regions of EPBs are filled by ambient rich plasma associated with MSTIDs. In our case the generation mechanism of enhanced bright region (anomaly) may be associated with the electric field reversal to confined latitudes which may have caused the diminishing of EPBs, which, however, needs further investigation.

4. Concluding Remarks

We report a peculiar EPB event in which zonal drifts show sharp longitudinal gradient within a narrow longitudinal zone of $\sim 5.4^\circ$ over the Indian region. Multi-instrument data suggests the following points to be the important features associated with this event.

- (1) The ionosonde F-layer observations reveal the possibility of seed perturbation prior to the ESF occurrence.
- (2) Though EPBs are generated due to wavelike seed, the later dynamics was controlled by the disturbance dynamo.
- (3) We observed zonal drift gradient in EPBs within a narrow longitude zone of $\sim 5.4^\circ$. The leading EPB1 exhibits eastward motion only while trailing EPB2 initially moves eastward and then exhibits westward drift. This westward drift could be attributed to disturbance electric field associated with the disturbance dynamo.
- (4) The effect of eastward drift is prominent toward dip equatorial region as compared to low latitude region. This constitutes latitudinal drift gradient in zonal drift of EPBs.

- (5) The diminishing of EPBs is observed during the event. Plausibly it is caused due to the interaction of EPBs with enhanced intensity region (anomaly) which is generated at the dip equator and then traveled altitudinally (latitudinally).

Data Availability Statement

Datasets used for this research are available in Zenodo data center (<http://doi.org/10.5281/zenodo.4727136>). The interplanetary magnetic field (IMF Bz), interplanetary electric field (IEF), Auroral Electrojet Indices (AE) and SymH can be accessed through CDAWEB (<https://cdaweb.gsfc.nasa.gov/cgi-bin/eval2.cgi>). The international quiet days are taken from WDC, Kyoto Japan (<http://wdc.kugi.kyoto-u.ac.jp/qddays/>).

Acknowledgments

The nightglow ASI campaign observations are carried out at Panhala hill station, India by Indian Institute of Geomagnetism (IIG), Navi Mumbai. The research work carried out by authors in IIG is funded by Department of Science and Technology (DST), Govt. of India, New Delhi. One of the authors O. B. Gurav is highly grateful to the Director, IIG for financial support through "Research Associateship". Lead author thanks Dr. V. L. Narayanan (Post doc fellow, University of Arctic (UiT), Tromsø, Norway) for providing necessary programs of equidistant projection of all-sky images. CADI observations are made at Tirunelveli by IIG. VHF radar (GIRI) observations are made by National Atmospheric Research Laboratory (NARL) at Gadanki. Authors thank Dr. A. K. Patra for providing GIRI data and his valuable suggestions.

References

- Abdu, M. A. (2012). Equatorial spread F/plasma bubble irregularities under storm time disturbance electric fields. *Journal of Atmospheric and Solar-Terrestrial Physics*, 75–76, 44–56. <https://doi.org/10.1016/j.jastp.2011.04.024>
- Abdu, M. A., Batista, I. S., Takahashi, H., MacDougall, J., Sobral, J. H., Medeiros, A. F., & Trivedi, N. B. (2003). Magnetospheric disturbance induced equatorial plasma bubble development and dynamics: A case study in Brazilian sector. *Journal of Geophysical Research*, 108(A12), 1–13. <https://doi.org/10.1029/2002ja009721>
- Buhari, S. M., Abdullah, M., Yokoyama, T., Otsuka, Y., Nishioka, M., Hasbi, A. M., et al. (2017). Climatology of successive equatorial plasma bubbles observed by GPS ROTI over Malaysia. *Journal of Geophysical Research: Space Physics*, 122, 2174–2184. <https://doi.org/10.1002/2016ja023202>
- Candido, C. M. N., Shi, J., Batista, I. S., Becker-Guedes, F., Correia, E., Abdu, M. A., et al. (2019). Postmidnight equatorial plasma irregularities on the June solstice during low solar activity - A case study. *Annales Geophysicae*, 37, 657–672. <https://doi.org/10.5194/angeo-37-657-2019>
- Chian, A. C. L., Abalde, J. R., Miranda, R. A., Borotto, F. A., Hysell, D. L., Rempel, E. L., & Ruffolo, D. (2018). Multi-spectral optical imaging of the spatiotemporal dynamics of ionospheric intermittent turbulence. *Scientific Reports*, 8(1), 1–15. <https://doi.org/10.1038/s41598-018-28780-5>
- Fejer, B. G., de Paula, E. R., González, S. A., & Woodman, R. F. (1991). Average vertical and zonal F region plasma drifts over Jicamarca. *Journal of Geophysical Research*, 96(A8), 13901–13906. <https://doi.org/10.1029/91ja01171>
- Ghodpage, R. N., Patil, P. T., Gurav, O. B., Gurubaran, S., & Sharma, A. K. (2018). Ionospheric response to major storm of 17th March 2015 using multi-instrument data over low latitude station Kolhapur (16.8°N, 74.2°E, 10.6°dip. Lat.). *Advances in Space Research*, 62(3), 624–637. <https://doi.org/10.1016/j.asr.2018.05.003>
- Gurav, O. B., Narayanan, V. L., Sharma, A. K., Ghodpage, R. N., Gaikwad, H. P., & Patil, P. T. (2019). Airglow imaging observations of some evolutionary aspects of equatorial plasma bubbles from Indian sector. *Advances in Space Research*, 64(2), 385–399. <https://doi.org/10.1016/j.asr.2019.04.008>
- Gurav, O. B., Sharma, A. K., Ghodpage, R. N., Nade, D. P., Chavan, G. A., Gaikwad, H. P., & Patil, P. T. (2018). Zonal drift velocity of equatorial plasma bubbles during ascending phase of 24th solar cycle using all-sky imager over Kolhapur, India. *Journal of Geophysical Research: Space Physics*, 123, 10266–10282. <https://doi.org/10.1029/2018ja025810>
- Huba, J. D., Wu, T. W., & Makela, J. J. (2015). Electrostatic reconnection in the ionosphere. *Geophysical Research Letters*, 42, 1626–1631. <https://doi.org/10.1002/2015gl063187>
- Kakad, B., Surve, G., Tiwari, P., Yadav, V., & Bhattacharyya, A. (2017). Disturbance dynamo effects over low-latitude F region: A study by network of VHF spaced receivers. *Journal of Geophysical Research: Space Physics*, 122, 5670–5686. <https://doi.org/10.1002/2016ja023498>
- Kelley, M. C. (1989). *The earth's ionosphere: Plasma physics and electrodynamics*. San Diego, CA: Academic Press.
- Kelley, M. C., Makela, J. J., de La Beaujardière, O., & Retterer, J. (2011). Convective ionospheric storms: A review. *Reviews of Geophysics*, 49, RG2003. <https://doi.org/10.1029/2010RG000340>
- Makela, J. J., & Otsuka, Y. (2011). Overview of nighttime ionospheric instabilities at low- and mid-latitudes: Coupling aspects resulting in structuring at the mesoscale. *Space Science Reviews*, 168, 419–440. <https://doi.org/10.1007/s11214-011-9816-6>
- Martinis, C., Baumgardner, J., Wroten, J., & Mendillo, M. (2018). All-sky-imaging capabilities for ionospheric space weather research using geomagnetic conjugate point observing sites. *Advances in Space Research*, 61(7), 1636–1651. <https://doi.org/10.1016/j.asr.2017.07.021>
- Mukherjee, S., & Patra, A. K. (2014). Parallel plate capacitor analogy of equatorial plasma bubble and associated fringe fields with implications to equatorial valley region irregularities. *Journal of Geophysical Research: Space Physics*, 119, 6631–6641. <https://doi.org/10.1002/2014JA020113>
- Narayanan, V. L., Gurubaran, S., & Emperumal, K. (2009). Imaging observations of upper mesospheric nightglow emissions from Tirunelveli (8.7°N). *Indian Journal of Radio and Space Physics*, 38, 150–158.
- Narayanan, V. L., Gurubaran, S., Emperumal, K., & Patil, P. T. (2013). A study on the night time equatorward movement of ionization anomaly using thermospheric airglow imaging technique. *Journal of Atmospheric and Solar-Terrestrial Physics*, 103, 113–120. <https://doi.org/10.1016/j.jastp.2013.03.028>
- Otsuka, Y., Shiokawa, K., & Ogawa, T. (2012). Disappearance of equatorial plasma bubble after interaction with mid-latitude medium-scale traveling ionospheric disturbance. *Geophysical Research Letters*, 39, 1–5. <https://doi.org/10.1029/2012gl052286>
- Patra, A. K., Chaitanya, P. P., Dashora, N., Sivakandan, M., & Taori, A. (2016). Highly localized unique electrodynamic and plasma irregularities linked with the 17 March 2015 severe magnetic storm observed using multitechnique common-volume observations from Gadanki, India. *Journal of Geophysical Research: Space Physics*, 121, 11518–11527. <https://doi.org/10.1002/2016ja023384>
- Patra, A. K., Srinivasulu, P., Chaitanya, P. P., Rao, M. D., & Jayaraman, A. (2014). First results on low-latitude E and F region irregularities obtained using the Gadanki Ionospheric Radar Interferometer. *Journal of Geophysical Research: Space Physics*, 119, 10276–10293. <https://doi.org/10.1002/2014ja020604>
- Patra, A. K., Taori, A., Chaitanya, P. P., & Sripathi, S. (2013). Direct detection of wavelike spatial structure at the bottom of the F region and its role on the formation of equatorial plasma bubble. *Journal of Geophysical Research: Space Physics*, 118, 1196–1202. <https://doi.org/10.1002/jgra.50148>

- Paulino, I., Medeiros, A. F., Buriti, R. A., Sobral, J. H. A., Takahashi, H., & Gobbi, D. (2010). Optical observations of plasma bubble westward drifts over Brazilian tropical region. *Journal of Atmospheric and Solar-Terrestrial Physics*, 72, 521–527. <https://doi.org/10.1016/j.jastp.2010.01.015>
- Pimenta, A. A., Fagundes, P. R., Bittencourt, J. A., Sahai, Y., Gobbi, D., Medeiros, A. F., et al. (2001). Ionospheric plasma bubble zonal drift: A methodology using OI 630 nm all-sky imaging systems. *Advances in Space Research*, 27, 1219–1224. [https://doi.org/10.1016/s0273-1177\(01\)00201-0](https://doi.org/10.1016/s0273-1177(01)00201-0)
- Sahai, Y., Abalde, J. R., Fagundes, P. R., Pillat, V. G., & Bittencourt, J. A. (2006). First observations of detached equatorial ionospheric plasma depletions using OI 630.0 nm and OI 777.4 nm emissions nightglow imaging. *Geophysical Research Letters*, 33, 1–5. <https://doi.org/10.1029/2005gl025262>
- Sau, S., Narayanan, V. L., Gurubaran, S., Ghodpage, R. N., & Patil, P. T. (2017). First observation of interhemispheric asymmetry in the EPBS during the St. Patrick's Day geomagnetic storm of 2015. *Journal of Geophysical Research: Space Physics*, 122, 6679–6688. <https://doi.org/10.1002/2017ja024213>
- Sharma, A. K., Gurav, O. B., Chavan, G. A., Gaikwad, H. P., Ghodpage, R. N., & Patil, P. T. (2017). Variation in occurrence of equatorial plasma bubbles (EPBs) using All Sky Imager from low latitude station Kolhapur (16.8°N, 74.2°E, 10.6° dip. Lat.). *Advances in Space Research*, 60(11), 2452–2463. <https://doi.org/10.1016/j.asr.2017.09.014>
- Sobral, J. H. A., de Castilho, V. M., Abdu, M. A., Takahashi, H., Paulino, I., Gaspardo, U. A. C., et al. (2011). Midnight reversal of ionospheric plasma bubble eastward velocity to westward velocity during geomagnetically quiettime: Climatology and its model validation. *Journal of Atmospheric and Solar-Terrestrial Physics*, 73, 1520–1528. <https://doi.org/10.1016/j.jastp.2010.11.031>
- Sridharan, R., Sekar, R., & Gurubaran, S. (1993). Two-dimensional high-resolution imaging of the equatorial plasma fountain. *Journal of Atmospheric and Terrestrial Physics*, 55(13), 1661–1665. [https://doi.org/10.1016/0021-9169\(93\)90170-4](https://doi.org/10.1016/0021-9169(93)90170-4)
- Sripathi, S., Abdu, M. A., Patra, A. K., & Ghodpage, R. N. (2018). Unusual generation of localized EPB in the dawn sector triggered by a moderate geomagnetic storm. *Journal of Geophysical Research: Space Physics*, 123, 9697–9710. <https://doi.org/10.1029/2018ja025642>
- Sripathi, S., Singh, R., Banola, S., Sreekumar, S., Emperumal, K., & Selvaraj, C. (2016). Characteristics of the equatorial plasma drifts as obtained by using Canadian Doppler ionosonde over southern tip of India. *Journal of Geophysical Research: Space Physics*, 121, 8103–8120. <https://doi.org/10.1002/2016ja023088>
- Taori, A., Dashora, N., Raghunath, K., Rusell, III, J. M., & Mlynczak, M. G., (2011). Simultaneous mesosphere, thermosphere-ionosphere parameter measurements over Gadanki (13.5°N, 79.2°E)- First results, *Journal of Geophysical Research*, 116, A07308. <https://doi.org/10.1029/2010JA016154>
- Taori, A., Jayaraman, A., & Kamalakar, V. (2013). Imaging of mesosphere–thermosphere airglow emissions over Gadanki (13.5°N, 79.2°E)—First results. *Journal of Atmospheric and Solar Terrestrial Physics*, 93, 21–28. <https://doi.org/10.1016/j.jastp.2012.11.007>
- Taori, A. & Sindhya, A. (2014). Measurements of equatorial plasma depletion velocity using 630 nm airglow imaging over a low-latitude Indian station. *Journal of Geophysical Research: Space Physics*, 118, 396–401. <https://doi.org/10.1002/2013JA019465>
- Tsunoda, R. T., Saito, S., & Nguyen, T. T. (2018). Post-sunset rise of equatorial F layer—or upwelling growth? *Progress in Earth & Planetary Sciences*, 5, 22. <https://doi.org/10.1186/s40645-018-0179-4>
- Xiong, C., Xu, J., Wu, K., & Yuan, W. (2018). Longitudinal thin structure of equatorial plasma depletions coincidentally observed by Swarm constellation and all-sky imager. *Journal of Geophysical Research: Space Physics*, 123, 1593–1602. <https://doi.org/10.1002/2017ja025091>